Physics of Plasmas | ARTICLE | pubs.aip.org/aip/pop

Anomalous resistivity and electron heating by lower hybrid drift waves inside reconnecting current sheets

Cite as: Phys. Plasmas **32**, 062114 (2025); doi: 10.1063/5.0271730
Submitted: 19 March 2025 · Accepted: 10 June 2025 ·
Published Online: 24 June 2025

Jongsoo Yoo,[1,a)] Hantao Ji,[1,2] Peiyun Shi,[1] Sayak Bose,[1] Jonathan Ng,[3] Li-Jen Chen,[4] and Masaaki Yamada[1]

AFFILIATIONS

[1]Princeton Plasma Physics Laboratory, Princeton, New Jersey 08540, USA
[2]Department of Astrophysical Sciences, Princeton University, New Jersey 08544, USA
[3]Department of Astronomy, University of Maryland, College Park, Maryland 20742, USA
[4]NASA Goddard Space Flight Center, Greenbelt, Maryland 20771, USA

Note: This paper is part of the Special Collection: Papers from the 66th Annual Meeting of the APS Division of Plasma Physics.
Note: Paper BI3 4, Bull. Am. Phys. Soc. **69** (2024).
[a)]Invited speaker. **Author to whom correspondence should be addressed:** jyoo@pppl.gov

ABSTRACT

Inside an electron diffusion region of laboratory reconnection experiments, the quasi-electrostatic lower hybrid drift wave (ES-LHDW) is observed when a significant guide field component is present. Through direct measurement of the anomalous drag term and quasilinear analysis, it is shown that ES-LHDW can account for approximately 20% of the mean reconnection electric field in a case with moderate guide field. This value exceeds the contribution from classical resistivity, which is around 10%. The effects of the Lorentz force term, often neglected for electrostatic waves, are crucial for the observed correlation between electric field and density fluctuations. Anomalous electron heating by the perturbed current and resistivity ($2.6\,\mathrm{MW/m^3}$) also surpasses the classical Ohmic heating, which is about $2.0\,\mathrm{MW/m^3}$. For the case with a high guide field, significantly higher local electron temperatures were observed during periods of strong ES-LHDW activity. A statistical analysis further supports electron heating by LHDW, showing a larger increase in electron temperature with a high guide field. Finally, data from the Magnetospheric Multiscale mission provide evidence of Landau damping of ES-LHDW, suggesting that ES-LHDW may contribute to the generation of nonthermal electrons along the direction parallel to the magnetic field.

I. INTRODUCTION

Magnetic reconnection is a fundamental process in which magnetic energy is rapidly converted into plasma energy through the rearrangement of magnetic topology.[1,2] This energy conversion generates several free energy sources for waves and instabilities near the diffusion region, such as strong gradients in the magnetic field and plasma parameters. These waves and instabilities can influence reconnection and plasma energization processes by introducing anomalous terms and contributing to kinetic dissipation.[3–5]

Among the various waves produced by magnetic reconnection, the lower hybrid drift wave (LHDW) has been frequently observed in the diffusion region, both in space[5–12] and laboratory plasmas.[13–16] The free energy source for LHDWs is the cross field current.[17] Notably, large density gradients near the separatrix provide a significant source of free energy by inducing a perpendicular current through diamagnetic drift.

LHDWs have been considered a potential mechanism for generating anomalous resistivity in the electron diffusion region, the central region of the reconnection process, as they can interact differently with magnetized electrons and non-magnetized ions, leading to momentum exchange between the two species.[12–14,18–22]

For reconnection in the absence of a guide field, the fast-growing, quasi-electrostatic LHDW (ES-LHDW) is typically localized at the edge of the current sheet,[13] stabilized by a high plasma beta (β).[23] In contrast, the electromagnetic LHDW (EM-LHDW), which propagates obliquely to the magnetic field, is found in the electron diffusion region.[14] However, numerical particle-in-cell (PIC) simulations[21,22] indicate that the EM-LHDW does not play a significant role in fast reconnection or electron energization near the electron diffusion region during antiparallel reconnection.

Recent space and laboratory observations[5,10–12,16,24] show that the ES-LHDW can be generated inside or near the electron diffusion region when there is a sizable guide field so that electron beta is low. The ES-LHDW has been found to generate an anomalous drag (resistivity) term inside the current sheet,[25]

$$D = -\frac{\langle \delta n_e \delta E_Y \rangle}{\langle n_e \rangle}, \tag{1}$$

where $\langle \ldots \rangle$ denotes a temporal average of a physical parameter, n_e is the electron density, δn_e is the electron density fluctuation, and δE_Y is the electric field fluctuation along the direction normal to the reconnection plane. Furthermore, LHDWs can influence electron dynamics by producing nongyrotropic heating and vortical flows,[11] as well as contributing to additional irreversible anomalous heating.[16] In addition, a statistical study with Magnetospheric Multiscale (MMS) data suggests that LHDW is related to electron heating in the downstream region.[26]

To explain these laboratory and space observations of LHDWs, two local, linear models have been developed: a collisionless model for space observations[12] and a collisional model for weakly collisional laboratory plasmas.[27] These models have successfully explained the stability and anomalous resistivity observed in both space and laboratory plasmas.

Here, we further explore the physics underlying anomalous resistivity and electron heating driven by ES-LHDWs, drawing on laboratory observations and theoretical analysis. Specifically, we decompose the contributions to anomalous resistivity and examine how these contributions vary for EM-LHDW. Additionally, we present laboratory observations of ES-LHDWs in the presence of a strong guide field and analyze how these observations account for the higher local electron temperature compared to cases with a moderate guide field.

II. EXPERIMENTAL SETUP AND LOCAL COORDINATES

To quantitatively address the impact of lower hybrid drift waves (LHDWs) on reconnection and electron dynamics, we conducted experiments using the Magnetic Reconnection Experiment (MRX). The MRX device consists of a cylindrical vacuum vessel with a diameter of 1.5 m and a height of approximately 2 m. Figure 1(a) shows a cross-sectional view of MRX in the RZ plane. A local Cartesian

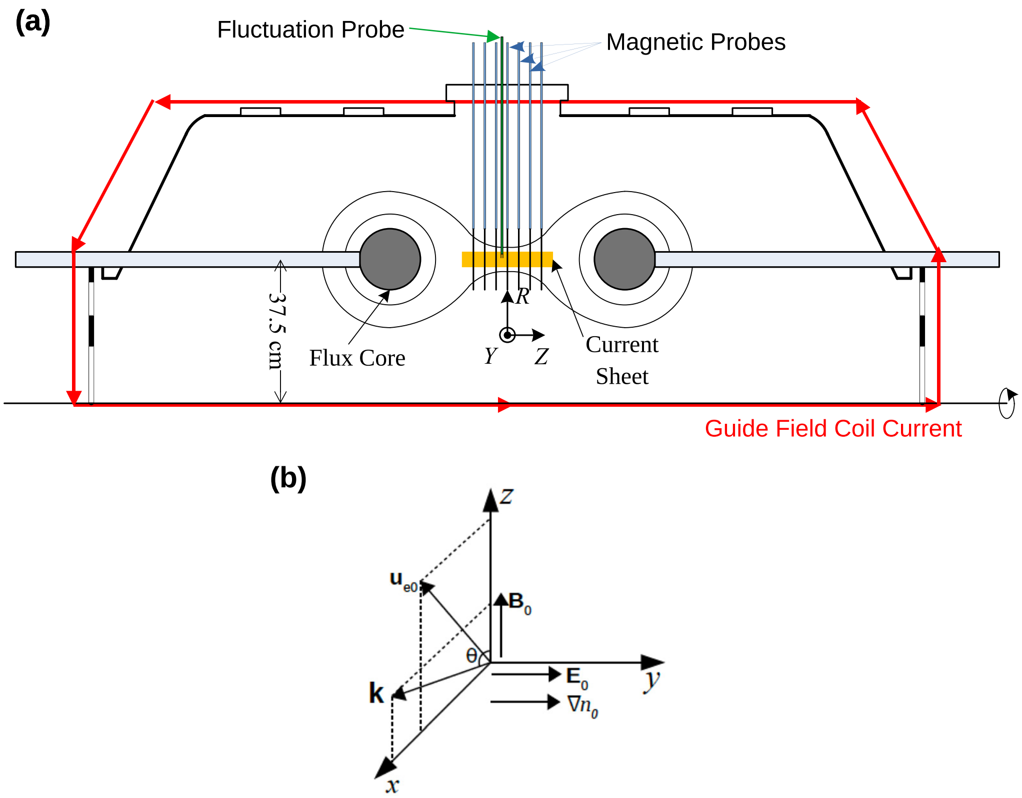

FIG. 1. (a) MRX apparatus. MRX has a cylindrical vacuum vessel and this shows a cutaway view of MRX. Two flux cores (gray circles) generate plasma and drive reconnection. The guide field coil generates a relatively uniform toroidal (out-of-plane) magnetic field. Equilibrium field coils control the radial location of the current sheet. The MRX coordinate system is based on (R, Y, Z), where Y is along the out-of-plane direction. (b) The local coordinate system (x, y, z) for the theoretical model. The z is along the magnetic field direction ($\mathbf{B_0}$), while y is along the density gradient direction. Both the wave vector $\mathbf{k}$ and the electron flow in this ion rest frame are on the xz plane. The angle between $\mathbf{B_0}$ and $\mathbf{k}$ is defined as θ. For cases with a strong guide field, the local wave coordinate system is approximately aligned as follows: the z-axis lies along the Y (guide field) direction, the x-axis is primarily along the electron outflow (Z) direction, and the y-axis is roughly aligned with the normal to the current sheet (R direction).

coordinate system is employed, where R represents the radial direction, Z the axial direction, and Y the toroidal direction.

The gray circles in the figure indicate doughnut-shaped flux cores, each containing independent coils that drive magnetic reconnection and generate plasma.[28] The primary diagnostic tool is a two-dimensional (2D) magnetic probe array consisting of approximately 250 miniature pickup coils.[15,29] Assuming toroidal symmetry, this probe array enables the reconstruction of two-dimensional profiles of the magnetic field (**B**), current density (**J**), and the reconnection electric field ($E_{\rm rec} = -E_Y$).

In addition to the main diagnostic, we have developed a special electrostatic probe that measures the electron density ($n_{\rm e}$) and temperature ($T_{\rm e}$) as well as high-frequency fluctuations in the electron density ($\delta n_{\rm e}$) and in the electric field along the reconnection electric field direction (δE_Y).[30] Data from this probe can be used to compute the anomalous resistivity term [D, Eq. (1)] as well as the classical resistivity term ($\eta_{\|} J_{\|} + \eta_{\perp} J_{\perp}$) with **J** and **B** measured by the magnetic probe array. As a result, a direct comparison between the anomalous and classical resistivity terms is possible.

The plasma in these experiments has a Lundquist number of approximately 300, and the system size, normalized to the ion sound radius, is about 20. These conditions place the plasma in the single X-line, collisionless reconnection regime.[2,31] Within the current sheet, the plasma is weakly collisional—collisional effects are present but negligible in influencing the reconnection dynamics.

Figure 1(b) illustrates the geometry of our local theoretical model for LHDWs within a current sheet. In this model, the subscript 0 denotes equilibrium quantities. We adopt the ion rest frame, where electrons move with velocity $\mathbf{u}_{\rm e0}$ in the $x - z$ plane. In this Cartesian coordinate system, the equilibrium magnetic field ($\mathbf{B}_0$) aligns with the z direction, while the equilibrium density gradient lies along the y direction.

The model assumes no equilibrium temperature gradient or ion temperature anisotropy. The equilibrium electron temperature is also assumed to be isotropic, although anisotropy is permitted in the perturbed electron temperature. The wave vector (**k**) is restricted to the $x - z$ plane due to the assumption of negligible k_y. Consequently, this theoretical model is local and applicable only when the wavelength of the LHDW is much smaller than the thickness of the current sheet in the y direction.[32]

The relationship between the two coordinate systems must be explained. First, it is important to emphasize that the local coordinate system (x, y, z) is in the ion rest frame. Since the ion flow speed in MRX is much lower than the speed of light, we will use a non-relativistic limit for computing physical quantities. In other words, we assume that the magnetic field in the ion rest frame is the same as the laboratory frame and the electron velocity in the ion rest frame such as $\mathbf{u}_{\rm e0}$ can be obtained by subtracting the ion velocity from the electron velocity.

Under this approximation, only three quantities need to be measured in the laboratory (R, Y, Z) frame to obtain the transformation matrix from one coordinate system to the other: the magnetic field $\mathbf{B}_0$, the current density $\mathbf{J}_0$, and the electron density n_0. Then, the electron velocity in the ion rest frame can be computed by $\mathbf{u}_{\rm e0} \approx -\mathbf{J}_0/(en_0)$ (ignoring relativistic effects, since the ion flow velocity is much smaller than the speed of light), where e is the elementary charge. With measured $\mathbf{B}_0$ and $\mathbf{u}_{\rm e0}$, the unit vector along the z direction ($\mathbf{e}_z$) becomes $\mathbf{B}_0/B_0$, $\mathbf{e}_y = \mathbf{B}_0 \times \mathbf{u}_{\rm e0}/|\mathbf{B}_0 \times \mathbf{u}_{\rm e0}|$, and $\mathbf{e}_x = \mathbf{e}_y \times \mathbf{e}_z$. With these unit vectors, the transformation matrix (**M**) from the (x, y, z) system to the (R, Y, Z) system is just $\mathbf{M} = [\mathbf{e}_x; \mathbf{e}_y; \mathbf{e}_z]$ and the transpose of **M** can be used to convert a tensor from the (R, Y, Z) system to the (x, y, z) system.

The method described above implies that the transformation matrix **M** depends strongly on local conditions, particularly the presence or absence of a guide field. As a result, there is no single transformation matrix that applies universally. However, we can describe the general orientation of the coordinate axes for two representative limiting cases.

In the high guide field case, the magnetic field near the electron diffusion region is predominantly toroidal (along the Y direction), so $\mathbf{e}_z$ is approximately aligned with Y. The perpendicular current is primarily due to electron outflows, which are directed along Z, making $\mathbf{e}_x$ roughly parallel to Z. Consequently, the density gradient direction $\mathbf{e}_y$ is aligned with the normal to the current sheet, along the R direction.

In the zero guide field case, the magnetic field aligns with the reconnecting field component, which lies along Z, so $\mathbf{e}_z$ is approximately in the Z direction. In this case, the perpendicular current is dominated by the out-of-plane component, aligning $\mathbf{e}_x$ with Y. As in the high guide field case, $\mathbf{e}_y$ remains along the R direction, normal to the current sheet.

III. RESULTS

A. Moderate guide field case

Figure 2 provides an overview of discharge 191 235, where the guide field ($B_{\rm g}$) is approximately 0.7 times of $B_{\rm rec}$. Here, $B_{\rm g}$ represents the absolute value of B_Y at the X-line, while $B_{\rm rec}$ refers to the strength of the reconnecting field component (B_Z) in the upstream region. In this discharge, the density asymmetry across the current sheet is around 2, resulting in minimal asymmetry in B_Z.[33] All presented data are obtained at $(R, Z) = (37.5, -1.5)$ cm except for the 2D plot shown in panel (i).

Figure 2(i) shows the profile of the out-of-plane current density (J_Y) at $t = 348\ \mu$s; in addition, the black lines are the contours of the poloidal magnetic flux, representing magnetic field lines.[15] The measurement location $(R, Z) = (37.5, -1.5)$ cm marked with a blue asterisk is inside the electron diffusion region (EDR) where the reconnection process takes place. In this discharge, the X-line is relatively stable for the presented period of time, providing an opportunity to study LHDWs in the EDR.

Fluctuations in E_Y and $n_{\rm e}$ are presented in panels (a) and (b), respectively. Notably, from $t = 347$ to $354\ \mu$s, these fluctuations exhibit strong correlation and are nearly in phase. The amplitude of δE_Y is ~ 150 V/m, which is about twice the mean reconnection electric field $\langle E_{\rm rec}\rangle$ of about 80 V/m. The amplitude of $\delta n_{\rm e}$ is $\sim 0.5 \times 10^{13}$ cm^{-3}, which is about 25% of the mean density $\langle n_{\rm e}\rangle$.

From these measured data, the anomalous drag term can be directly estimated. With the measured phase difference of approximately 30°, the drag term is given by $D \approx -0.5|\delta n_{\rm e}||\delta E_Y|/\langle n_{\rm e}\rangle \cos 30°$ ≈ 16 V/m, which accounts for about 20% of the average reconnection electric field. This value also exceeds the contribution from classical resistivity, estimated as $\sim \eta_{\|} J_{\|} \sim 7$ V/m. Here, $\eta_{\|}$ and $J_{\|}$ represent the parallel Spitzer resistivity and the parallel current density, respectively. Near the electron diffusion region, the magnetic field is primarily aligned along the Y direction due to the presence of a sizable guide field.

Panels (c) and (d) show the time evolution of electron density ($n_{\rm e}$) and electron temperature ($T_{\rm e}$), respectively, measured by the same probe. As $n_{\rm e}$ decreases from 4×10^{13} to about 2×10^{13} cm^{-3},

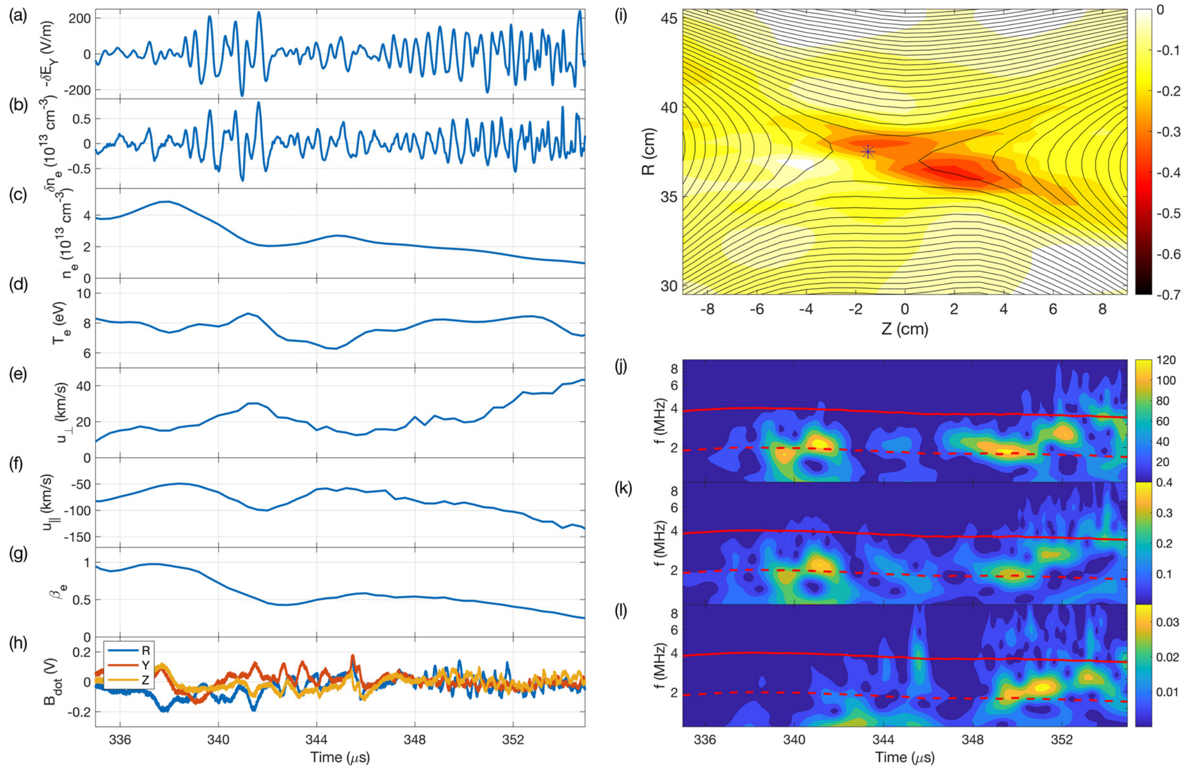

FIG. 2. Overview of MRX helium discharge 191 235 with a moderate guide field ($B_g/B_{rec} \sim 0.7$). The measurement location is $(R, Z) = (37.5, -1.5)$, which is marked with a blue asterisk in panel (i). (a) Fluctuations in the reconnection electric field measured by a fluctuation probe in the electron diffusion region. (b) Fluctuations in the electron density (in the unit of 10^{13} cm^{-3}) measured by the same fluctuation probe. There is strong correlation between $-\delta E_Y$ and δn_e. (c) Electron density (n_e) measured by the same probe. (d) Electron temperature (T_e) measured by the same probe. (e) Perpendicular component of the relative velocity between electrons and ions. (f) Parallel component of the relative velocity between electrons and ions. (g) Electron beta (β_e) at the measurement location. (h) All three component of magnetic fluctuations measured by a magnetic fluctuation probe, which is separated by 3 cm along the Y direction. (i) Profile of the out-of-plane current density (color contours with the unit of MA/m^2) with the poloidal flux lines representing magnetic field lines at $t = 348\ \mu$s. The blue asterisk indicates the location of two fluctuation probes. (j) Spectrogram of the electric field (E_Y) fluctuation. The red line indicates the local lower hybrid frequency, f_{LH}, while the red dashed line denotes $0.5f_{LH}$. (k) Spectrogram of the density fluctuation. (l) Spectrogram of the magnetic field (B_Z) fluctuation.

correlated fluctuations in E_Y and n_e emerge. This behavior is linked to the value of β_e [panel (g)]; when β_e is high, the electrostatic lower-hybrid drift wave (ES-LHDW) transitions into a relatively slow-growing electromagnetic lower-hybrid drift wave (EM-LHDW). Notably, during the period with the correlated fluctuations ($t = 347$–354), the local electron temperature remains relatively high (~ 8 eV), compared to the base electron temperature of about 6 eV, suggesting possible electron heating associated with these fluctuations.

The perpendicular and parallel components of the electron flow velocity in the ion rest frame are shown in panels (e) and (f), respectively. It is interesting to observe that $u_\perp$ remains low (< 20 km/s) during the brief period of relatively low LHDW activity ($t = 343$–347). This behavior is consistent with the understanding that $u_\perp$ represents the free energy source for LHDWs. The parallel component of the electron flow is substantial, driven by the presence of u_{eY} and B_Y (guide field). The parallel component has a relatively small effect on the overall stability of the dispersion relation but influences the location of the maximum growth rate and frequency.

The time evolution of β_e is shown in panel (g). Initially, β_e is high (around 1), but as it decreases below 0.5, ES-LHDW activity [panels (a) and (b)] becomes more pronounced. The nature of the waves—whether quasi-electrostatic or electromagnetic—primarily depends on β_e,[12] though the available free energy also plays a role.

For comparison, magnetic field fluctuations are shown in panel (h). The signals come from a separate fluctuation probe positioned at the same R and Z coordinates; however, the two fluctuation probes are offset by 4 cm along the Y direction. The magnetic fluctuation probe detects fluctuations in all three components of the magnetic field up to 200 MHz (Ref. 34) using small pickup coils. The data in panel (h) represent the raw signals from these coils, which are proportional to the temporal changes in magnetic field. Notably, magnetic field fluctuations are observed in conjunction with the correlated electric field and density fluctuations between $t = 348$ and $352\ \mu$s. This indicates that the ES-LHDW is not purely electrostatic; in addition to the significant electric field fluctuations, it is capable of generating magnetic field fluctuations through the perturbed current density.

Finally, spectrograms of δE_Y, δn_e, and δB_Z are presented in panels (j), (k), and (l), respectively. The red solid lines denote the local lower hybrid frequency, $f_{LH} = \sqrt{f_{ce} f_{ci}}$, where f_{ce} and f_{ci} represent the electron and ion cyclotron frequencies, respectively. The red dashed lines correspond to $0.5f_{LH}$. The observed fluctuations between $t = 347$ and $354\ \mu$s are primarily concentrated around $0.5f_{LH}$.

To confirm that the observed wave activity is associated with ES-LHDW, the dispersion relation is calculated using the measured plasma and magnetic field parameters. The values used are $T_e = T_i = 7.9\,\mathrm{eV}$, $n_0 = 2 \times 10^{13}\,\mathrm{cm}^{-3}$, $B_0 = 110$ Gauss, $u_{e0z} = -83\,\mathrm{km/s}$, $u_{e0x} = 23\,\mathrm{km/s}$, and $\mu = m_i/m_p = 4$, where m_i is the ion mass and m_p is the proton mass. The dispersion relation is obtained using a linear model for weakly collisional plasmas.[27] This model computes the complex wave frequency for a given k and θ [$\omega(k,\theta)$] in the ion rest frame. As a local model, it neglects effects from the global structure of the current sheet, assuming no wave propagation along the density gradient. Using the aforementioned field and plasma parameters, the dispersion relation of LHDW is obtained. The transformation matrix (**M**) is given by

$$\begin{pmatrix} x \\ y \\ z \end{pmatrix} = \begin{pmatrix} 0.4233 & -0.0375 & -0.9062 \\ 0.9060 & 0.0202 & 0.4228 \\ 0.0024 & -0.9991 & 0.0420 \end{pmatrix} \begin{pmatrix} R \\ Y \\ Z \end{pmatrix}, \qquad (2)$$

which suggests that the gradient (y) direction is mostly along the R direction.

The real and imaginary parts of $\omega(k,\theta)$, normalized to ω_{LH}, are shown in Figs. 3(a) and 3(b), respectively. The model predicts that ES-LHDW is unstable near the X-line with a maximum growth rate of $0.2\omega_{\mathrm{LH}}$ at $(k\rho_e, \theta) = (0.63, 90°)$. Here, ρ_e is the local electron gyro radius. In the lab frame, this indicates that the wave predominantly propagates along the electron outflow [Eq. (2)], which is consistent with recent simulations.[35] The real frequency with the maximum growth rate is about $0.27\,\omega_{\mathrm{LH}}$, which is different from the observed frequency of $\sim 0.5\omega_{\mathrm{LH}}$. This discrepancy arises from the frame difference, as the model is in the ion rest frame. Accounting for the measured ion flow of 5 km/s along the $-Z$ direction in similar discharges, the frequency of LHDW shifts to $\sim 0.5\omega_{\mathrm{LH}}$ in the lab frame, consistent with the measured frequency.

We also confirm that the linear relationship between δn_e and δE_Y predicted by the model aligns with experimental measurements. As shown in Fig. 3(c), the reconstructed δn_e (red dashed line) closely matches the measured δn_e (blue line) in both amplitude and phase. This agreement indicates that the observed ES-LHDW operates in the linear regime, allowing other anomalous terms to be estimated using the model's linear relationship.

The reconstruction process of δn_e from δE_Y follows a specific approach. Within this linear model, all quantities, including δn_e, can be expressed as a function of δE_Y with a complex coefficient A: $\delta n_e(k,\theta) = -A(k,\theta)\delta E_Y(k,\theta)$. This coefficient, which defines the linear relationship between the two fluctuating quantities, depends on both k and θ. A direct comparison requires knowledge of $\delta E_Y(k,\theta)$ for all modes, which is impractical since δE_Y is typically expressed as a function of frequency through Fourier transformation. However, given that wave energy is predominantly concentrated around $0.5 f_{\mathrm{LH}}$ and that A varies only weakly with k and θ near the maximum growth rate, it is reasonable to approximate $\delta E_Y(f)$ using the coefficient at the mode with the highest

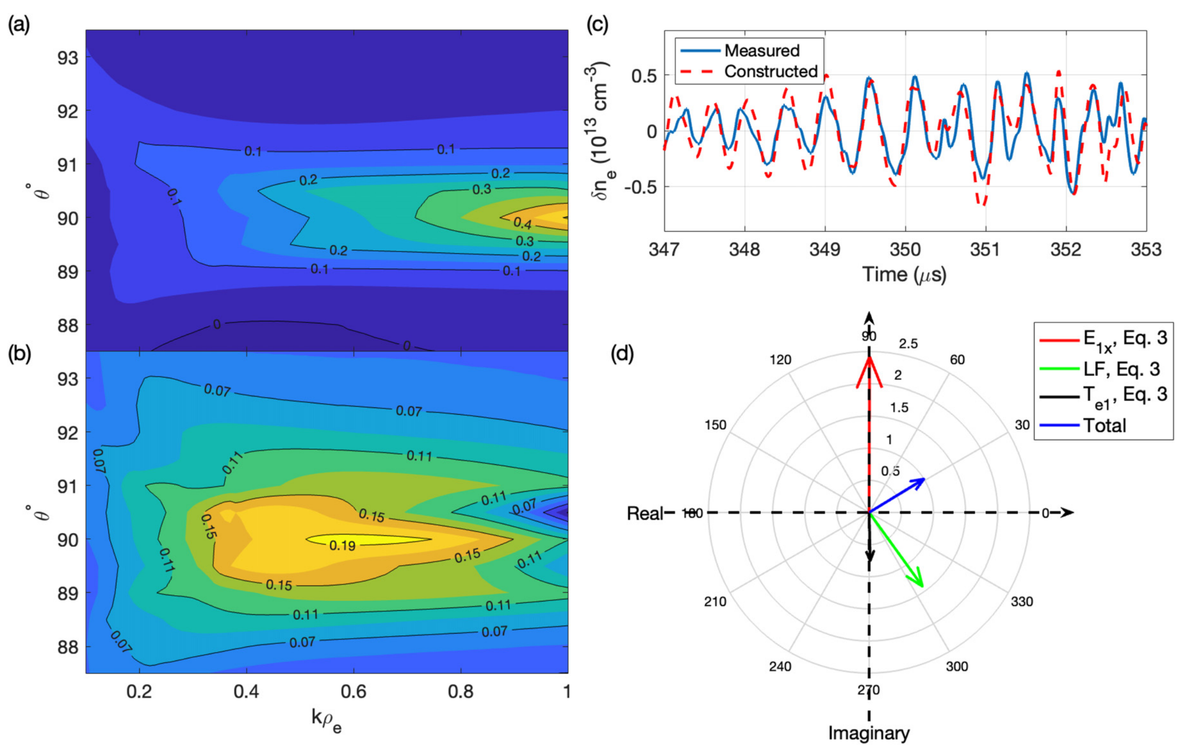

FIG. 3. (a) Real part of the angular frequency as a function of $k\rho_e$ and θ, normalized to ω_{LH}. (b) Growth rate, also normalized to ω_{LH} as a function of $k\rho_e$ and θ. The theoretical model expects a strong growth rate of approximately $0.2\,\omega_{\mathrm{LH}}$ at $(k\rho_e, \theta) = (0.63, 90°)$. (c) Comparison of the measured (blue solid line) and reconstructed (red dashed line) density fluctuations. The reconstruction is based on the measured δE_Y and the linear relation from the collisional model, showing good agreement in both amplitude and phase. (d) Breakdown of the contribution of each term to the normalized density fluctuation ($\delta n_e/n_e$) of the x component of the electron momentum equation, displayed on the complex plane. The only term that has a significant real part is the Lorentz force term. The contribution from the resistivity and inertial terms in Eq. (3) is too small.

growth rate, $A(k_{\max}, \theta_{\max})$. The reconstructed δn_e is then obtained by applying the inverse Fourier transform to $A(k_{\max}, \theta_{\max})\delta E_Y(f)$.

Both theoretical and experimental results indicate that ES-LHDW can generate anomalous resistivity. To investigate the underlying physics, we examine the x component of the first-order electron momentum equation, which can be expressed in terms of the normalized electron density fluctuation,[27]

$$\frac{\delta n_e}{n_e} = \frac{ie}{k_\perp T_{e0}}\delta E_x + \left(\frac{ieB_0}{k_\perp T_{e0}}\delta u_{ey} - \frac{ieu_{e0z}}{k_\perp T_{e0}}\delta B_{1y}\right) - \frac{\delta T_e}{T_{e0}} + \frac{m_e(\omega - \mathbf{k}\cdot\mathbf{u}_{e0})}{k_\perp T_{e0}}\delta u_{ex} - \frac{i\delta R_{e1x}}{k_\perp n_0 T_{e0}}, \quad (3)$$

where i is the unit imaginary number, $k_\perp$ is the perpendicular component of $\mathbf{k}$, δR_{e1x} is the x component of the first-order resistivity. Each term on the right-hand side corresponds to the contributions from the electric field, Lorentz force, perturbed temperature, internal forces, and resistivity, respectively. In the electrostatic limit with no perturbed electron temperature ($\delta T_e = 0$), as in the case of a Langmuir wave, the electric field term balances the density fluctuation. Here, the density and electric field fluctuations are out of phase due to the presence of i in the coefficient of δE_x. By analyzing the contributions from the remaining terms, we can identify the primary mechanism responsible for the anomalous resistivity observed in our experiments.

Figure 3(d) illustrates the contribution of each term to the normalized density fluctuation. All first-order quantities in Eq. (3) are expressed in terms of δE_Y, and the complex coefficient of each term is plotted on the complex plane. The term with a significant real component is responsible for the observed anomalous resistivity. The blue arrow represents the complex coefficient A in $\delta n_e/n_e = A\delta E_Y$. As expected, the electric field term is dominated by its imaginary component, while both the inertial and resistivity terms are negligible. The only term with a significant real component is the Lorentz force term (green arrow), highlighting its crucial role in understanding this quasi-electrostatic LHDW. Although ES-LHDW exhibits large electric field fluctuations, its underlying physics cannot be fully understood without accounting for this often-overlooked electromagnetic term[23,36] for electrostatic waves. Additionally, the perturbed temperature term (black arrow) enhances the correlation between δn_e and δE_Y by reducing the imaginary component.

B. High guide field case

Figure 4 provides an overview of the MRX helium discharge 191 002, representing a case where the guide field strength is

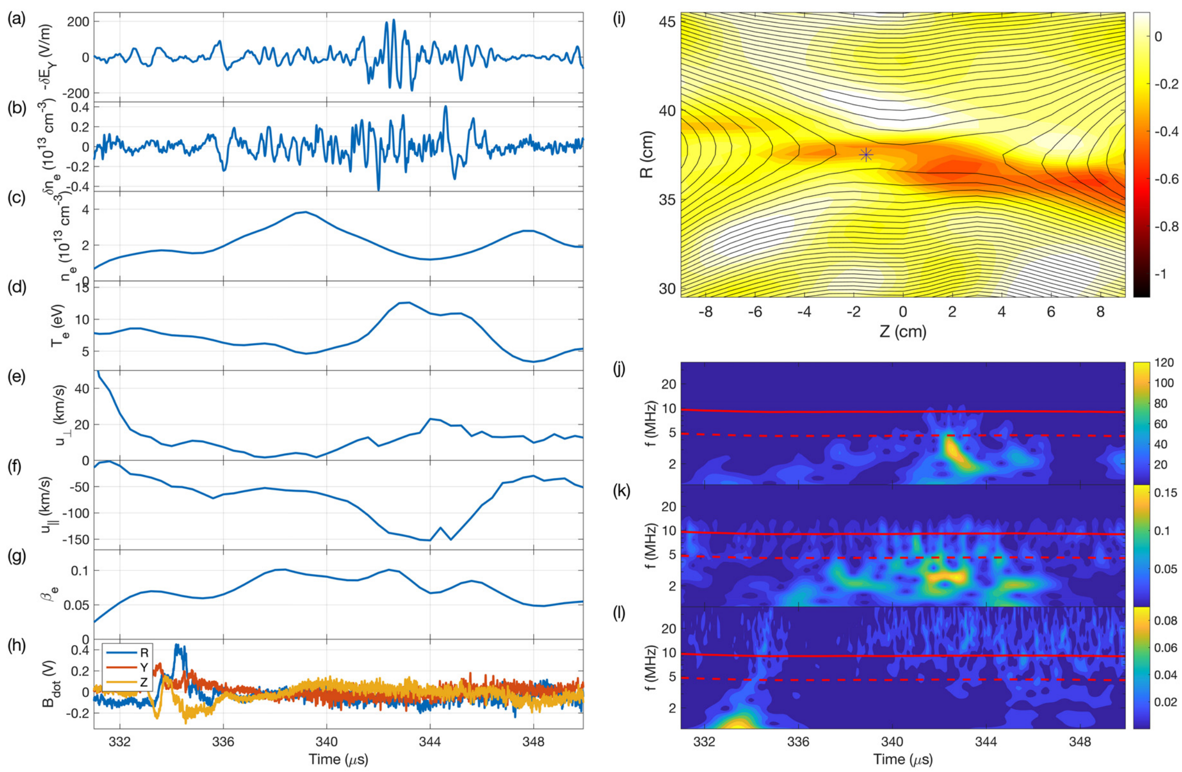

FIG. 4. Overview of MRX helium discharge 191 002 with a high guide field ($B_g/B_{rec} \sim 2$). The measurement location is $(R, Z) = (37.5, -1.5)$ cm, which is marked with a blue asterisk in panel (i). (a) Fluctuations in the reconnection electric field measured by a fluctuation probe in the electron diffusion region. (b) Fluctuations in the electron density (in the unit of 10^{13} cm^{-3}) measured by the same fluctuation probe. (c) Electron density (n_e) measured by the same probe. (d) Electron temperature (T_e) measured by the same probe. (e) Perpendicular component of the relative velocity between electrons and ions. (f) Parallel component of the relative velocity between electrons and ions. (g) Electron beta (β_e) at the measurement location. (h) All three component of magnetic fluctuations measured by a magnetic fluctuation probe, which is separated by 3 cm along the Y direction. (i) Profile of the out-of-plane current density (color contours with the unit of MA/m^2) with the poloidal flux lines representing magnetic field lines at $t = 342.4$ μs. The blue asterisk indicates the location of two fluctuation probes. (j) Spectrogram of the electric field (E_Y) fluctuation. The red line indicates the local lower hybrid frequency, f_{LH}, while the red dashed line denotes $0.5f_{LH}$. (k) Spectrogram of the density fluctuation. (l) Spectrogram of the magnetic field (B_Z) fluctuation.

approximately twice that of the reconnecting field component. The measurement location, $(R, Z) = (37.5, -1.5)$ cm, lies within the EDR, as indicated in panel (i). This discharge serves as a useful comparison to previous cases with moderate guide fields, allowing us to examine how increased guide field strength influences wave activity, correlations, and electron heating.

In this high guide field case, the correlation between δE_Y and δn_e weakens compared to the moderate guide field case, as shown in panels (a) and (b). This suggests that the coupling between electric field fluctuations and density perturbations becomes less effective when the guide field is strong. Additionally, the fluctuation spectrum broadens, as seen in panels (j) and (k), indicating the presence of a wider range of wave modes. Consequently, instances where fluctuation amplitudes exceed 200 V/m become increasingly rare. In contrast, at moderate guide field strengths, large-amplitude fluctuations (>200 V/m) were observed more frequently. This suggests that at higher guide fields, wave energy is distributed more evenly across multiple modes rather than being concentrated in a few dominant ones, leading to an earlier onset of nonlinear behavior. The underlying cause of this difference in nonlinear LHDW behavior remains an open question and requires further investigation.

Another key observation is the pronounced electron heating associated with strong fluctuations, as shown in panel (d). While the baseline electron temperature remains similar in both the moderate and high guide field cases (5–7 eV), localized electron heating is significantly more intense in the high guide field case, with temperatures reaching up to 12 eV.

Finally, as shown in panel (l), magnetic field fluctuations corresponding to whistler waves[37] are observed at frequencies exceeding $f_{\rm LH}$. Notably, in many high guide field cases, magnetic fluctuations associated with LHDW are relatively weak or absent. This suggests that under high guide field conditions, whistler waves may become the dominant magnetic fluctuation mode, potentially due to different excitation mechanisms, such as temperature anisotropy with higher parallel than perpendicular temperature[34,38] or modifications in electron dynamics within the EDR due to strong magnetization. Further investigation is needed to clarify this behavior.

C. Anomalous electron heating

The two previous examples suggest a potential link between ES-LHDW and electron heating, as localized electron temperature increases when fluctuation amplitudes are large. To further investigate this trend, a statistical analysis has been performed.

Figure 5 presents results from approximately 200 helium discharges conducted under identical operational conditions, including operation voltage, stored energy, and gas fill pressure, while varying the guide field strength. In all cases, the probe was positioned within 2 cm ($\sim 10 d_e$, where d_e is the electron skin depth) of the X-line, and both T_e and $|\delta E_Y|$ were averaged over 1.6 μs. There was no significant variation in the baseline electron temperature in the upstream region or in the reconnection electric field. The dataset is divided into two groups: blue asterisks represent data from reconnection events with a moderate guide field ($B_g/B_{\rm rec} \sim 0.7$, including discharge 191 235), while red asterisks correspond to reconnection events with a high guide field ($B_g/B_{\rm rec} \sim 2$, including discharge 191 002). In both cases, a statistically significant (p-value $\lesssim 10^{-5}$) and moderate correlation (coefficient ~ 0.5) is observed between T_e and $|\delta E_Y|$, reinforcing the hypothesis that ES-LHDW contributes to electron heating within the current sheet.

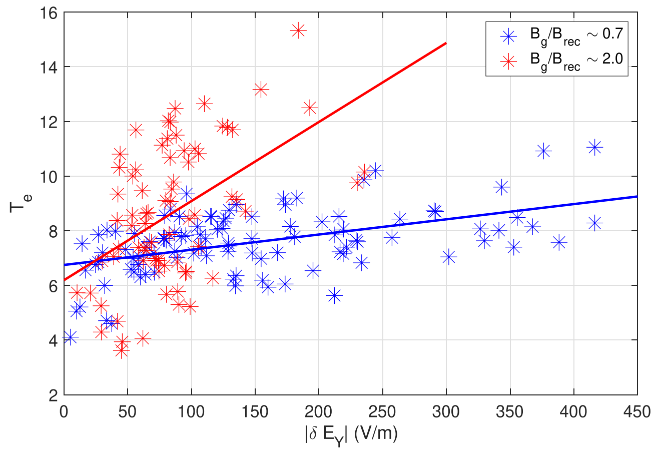

FIG. 5. Electron temperature as a function of the amplitude ($|\delta E_Y|$) of LHDW near the X-line for both moderate (blue asterisks) and high (red) guide field cases. Solid lines indicate the fit of data to a linear function. In both cases, the correlation coefficient is about 0.5 with a negligible probability value of the null hypothesis ($\lesssim 10^{-5}$). These values mean moderate correlation and strong statistical significance.

Notably, electron heating is more pronounced in the high guide field case, whereas $|\delta E_Y|$ exhibits larger amplitudes in the moderate guide field case, consistent with the previously discussed examples. When $|\delta E_Y|$ reaches 200 V, the expected electron temperature increase is approximately 6 eV in the high guide field case, compared to only 1 eV in the moderate guide field case. One possible explanation for this enhanced electron heating in the high guide field case is that broadband fluctuations more efficiently interact with electrons either via Landau damping or anomalous electron heating, facilitating stronger energy transfer in a high guide field environment. Additionally, the stronger guide field may lead to improved local heat confinement, further contributing to the observed high electron temperature.[39]

Anomalous electron heating due to ES-LHDW can be quantified through quasilinear analysis. For discharge 191 235, we have confirmed that the linear relationship predicted by the weakly collisional model[27] remains valid despite the large wave amplitude. Assuming that this linear relation also holds for other relevant quantities, the additional electron heating induced by ES-LHDW can be estimated using a quasilinear approach.[18] It is important to note that the weakly collisional model accounts for all Coulomb collision-related effects.

The anomalous electron heating rate can be expressed as $\langle \delta \mathbf{J}_e \cdot \delta \mathbf{R} \rangle$, where $\delta \mathbf{J}_e$ represents the first-order electron current and $\delta \mathbf{R}$ denotes the first-order drag force (resistivity). Physically, this heating arises from the work done by electrons as they move against the frictional force $\mathbf{R}$. After neglecting the negligible contribution of temperature fluctuations to $\delta \mathbf{R}$, the estimated anomalous electron heating rate is approximately 2.6 MW/m^3 for $|\delta E_Y| \sim 150$ V/m. This value surpasses the classical Ohmic heating rate of $\eta_\parallel J_\parallel^2 + \eta_\perp J_\perp^2 \sim 2.0$ MW/m^3, highlighting the significance of this additional heating mechanism.

This anomalous heating is still irreversible like the classical Ohmic heating, as it arises from Coulomb collisions between electrons and ions. In addition to collisional heating, ES-LHDW can also contribute to electron heating through Landau damping,[40] which plays a crucial role in energy dissipation and redistribution within the plasma. However, quantifying heating via Landau damping requires direct

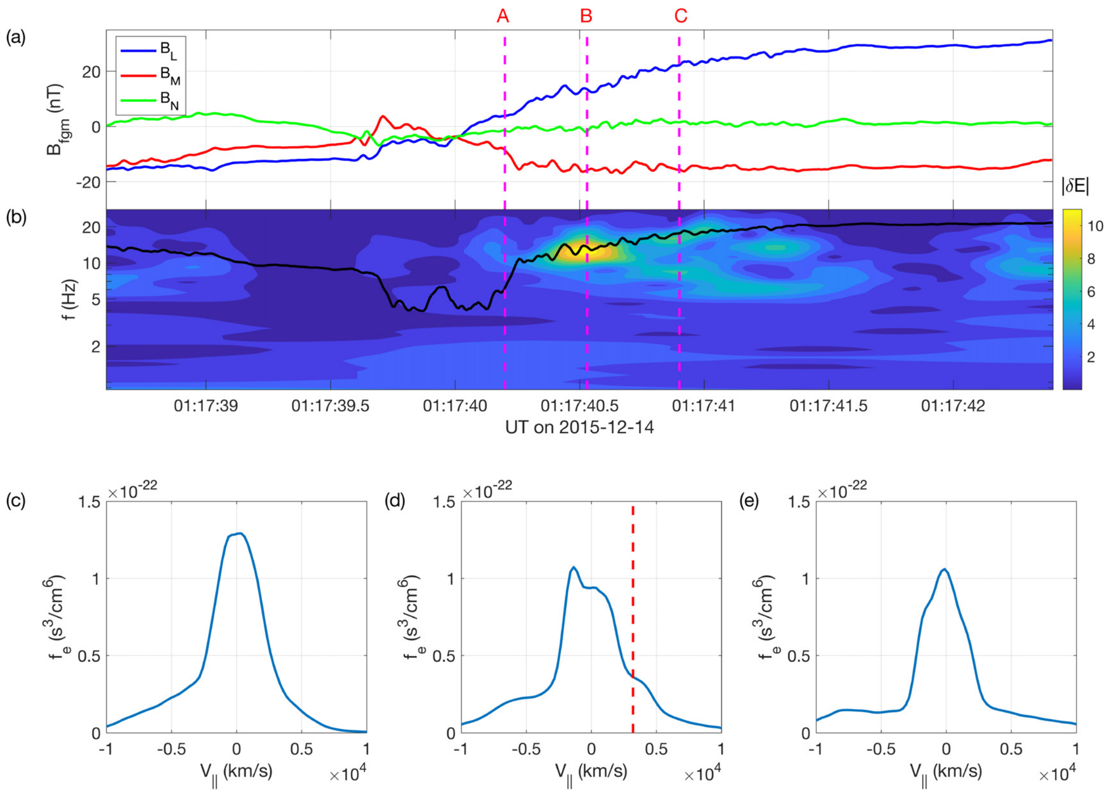

FIG. 6. (a) Magnetic field profile measured by MMS2 during a magnetopause reconnection event. The satellite is located near the electron diffusion region (EDR) around 01:17:40 UT on December 14, 2015. (b) Spectrogram of the electric field obtained via wavelet analysis. The black solid line denotes the local lower hybrid frequency (f_{LH}). Strong electric field fluctuations observed around 01:17:40.5 UT are associated with electrostatic lower hybrid drift waves (ES-LHDWs). The three magenta dashed lines mark the times at which electron distribution functions are analyzed. (c) Parallel electron distribution function at Region A (prior to strong ES-LHDW activity). (d) Parallel electron distribution function at Region B (during strong ES-LHDW activity). The vertical red dashed line indicates the predicted parallel phase velocity from collisionless linear theory. A clear flattening near this velocity provides strong evidence of Landau damping. (e) Parallel electron distribution function at Region C (after strong ES-LHDW activity), where the damping signature has subsided.

measurements of the electron distribution function, which are not available in the present laboratory experiments.

To overcome the limitations of laboratory measurements, we turn to data from NASA's Magnetospheric Multiscale (MMS) mission, which provides high-resolution electron distribution measurements with a temporal resolution of 30 ms.[41] Figure 6(a) shows the magnetic field profile during a magnetopause reconnection event, measured by MMS2 (Ref. 12) in the *LMN* coordinate system, where *L* is the outflow direction (analogous to *Z* in MRX), *M* is the out-of-plane direction (*Y* in MRX), and *N* is the current sheet normal (*R* in MRX). MMS was located near the EDR at approximately 01:17:40 UT. ES-LHDW is observed slightly away from the EDR on the low-density side.

Figure 6(b) displays the electric field spectrogram during the same interval, with the black curve indicating the local lower-hybrid frequency f_{LH}. Around 01:17:40.5 UT, strong electric field fluctuations are observed. Previous linear analysis and wave vector measurements confirm that these fluctuations are associated with electrostatic lower-hybrid drift waves (ES-LHDWs).[12] The wave phase velocity parallel to the magnetic field for the mode with maximum growth is estimated to be approximately 3200 km/s. As ES-LHDWs primarily interact with electrons along the magnetic field, we examine the parallel electron distribution function for signs of Landau damping.

To identify possible Landau damping signatures, we analyze the electron distribution at three times marked A, B, and C in panel (a). Notably, strong electric field fluctuations are observed only in region B. The one-dimensional distribution function is obtained by integrating the measured 3D distribution over two perpendicular velocity components.

In region A, prior to strong LHDW fluctuations, the parallel distribution function shows no evidence of Landau damping, as seen in panel (c). Here, $V_{||}$ denotes the parallel velocity, which corresponds to V_z in the local *xyz* coordinate system used in Fig. 1(b). In region B [panel (d)], clear flattening of the distribution function is observed near the wave phase velocity (indicated by the red dashed line), consistent with Landau damping by ES-LHDW. Finally, in region C [panel (e)], this flattening disappears, suggesting that the damping and associated heating were localized in time and space. These observations support electron heating via Landau damping of ES-LHDWs.

IV. DISCUSSION

We present the first quantitative laboratory results showing that the quasi-electrostatic lower-hybrid drift waves (ES-LHDWs) contribute to anomalous resistivity and electron heating inside the electron diffusion region.[16] The observed anomalous resistivity and anomalous electron heating cannot be explained without considering the Lorentz force term that is often neglected for electrostatic waves.

The measured anomalous resistivity typically contributes 10%–25% of the reconnection electric field in the moderate guide field case, while it decreases to about 5%–10% in the high guide field case. Given that the classical resistivity term generally accounts for approximately 10% of the reconnection electric field, this leaves 70%–80% of the reconnection electric field unaccounted for. The remaining portion must be balanced by other kinetic effects, such as the nongyrotropic pressure tensor,[41–43] or by additional anomalous contributions from higher-frequency fluctuations.

It is worth noting that the same quasilinear analysis indicates a minimal contribution (less than 1% of the mean reconnection electric field) from the anomalous viscosity term, which is known to counteract the effects of anomalous resistivity.[5] This cancelation relies on the frozen-in condition of electrons; however, this condition may not hold within the electron diffusion region. At this stage, drawing definitive conclusions about the role of anomalous viscosity remains challenging due to the absence of direct measurements of the necessary fluctuations in laboratory experiments. To further investigate this, we plan to conduct both linear and quasilinear analyses of ES-LHDW for the same MMS event reported by Graham *et al.*[5] Additionally, we aim to identify an event where ES-LHDW occurs inside the EDR and perform the same analysis to assess its impact in this critical region.

Another important finding is that electron heating by ES-LHDW exceeds classical Ohmic electron heating, even without considering collisionless Landau damping. The estimated term, $\langle \delta \mathbf{J}_e \cdot \delta \mathbf{R} \rangle$, represents additional irreversible heating of bulk electrons. Moreover, Landau damping could contribute to further electron energization. In the case of a moderate guide field, the linear model predicts that ES-LHDW has a small $k_\parallel$, allowing it to resonate with tail electrons and potentially generate nonthermal electron populations. This suggests that ES-LHDW can provide both thermal heating and the production of energetic electrons. Data from MMS show clear evidence of Landau damping by ES-LHDW (Fig. 6).

Another future research topic is to study the effects of EM-LHDW on electron heating and reconnection, which is typically considered negligible under symmetric and asymmetric anti-parallel reconnection parameters.[21,22] However, since we find that ES-LHDW and EM-LHDW are not distinct modes but rather the same mode with different wave characteristics depending on electron beta,[12,24] this suggests that EM-LHDW is not necessarily incapable of generating anomalous resistivity[18] and electron heating which was observed during EM-LHDW on MRX.[14] It will be interesting to investigate under what conditions LHDW loses its ability to generate anomalous resistivity and contribute to electron heating. Initial research suggests that this behavior is largely tied to a reduction in the magnitude of the electric field fluctuations. In other words, EM-LHDW can still influence electron heating and reconnection dynamics if it grows to a sufficiently large amplitude to generate strong electric field fluctuations. However, this is energetically challenging due to the substantial energy required to induce magnetic field fluctuations.

ACKNOWLEDGMENTS

This work was supported by DOE Contract No. DEAC0209CH11466, NASA Grant Nos. NNH20ZDA001N, 80HQTR21T0060, 80NSSC21K1462, 80NSSC21K1795, and 80HQTR21T0105, and the NASA MMS Project.

AUTHOR DECLARATIONS

Conflict of Interest

The authors have no conflicts to disclose.

Author Contributions

Jongsoo Yoo: Conceptualization (lead); Data curation (lead); Formal analysis (lead); Funding acquisition (lead); Investigation (lead); Methodology (lead); Project administration (equal); Visualization (lead); Writing – original draft (lead); Writing – review & editing (equal). **Hantao Ji:** Investigation (supporting); Methodology (supporting); Project administration (equal); Supervision (lead); Writing – review & editing (equal). **Peiyun Shi:** Investigation (supporting); Writing – review & editing (equal). **Sayak Bose:** Investigation (supporting); Writing – review & editing (equal). **Jonathan Ng:** Investigation (supporting); Writing – review & editing (equal). **Li-Jen Chen:** Investigation (supporting); Writing – review & editing (equal). **Masaaki Yamada:** Investigation (supporting); Writing – review & editing (equal).

DATA AVAILABILITY

The data that support the findings of this study are openly available in the Princeton Data Commons at https://doi.org/10.34770/hrkt-rw14, Ref. 44.

REFERENCES

[1] M. Yamada, R. Kulsrud, and H. Ji, "Magnetic reconnection," Rev. Mod. Phys. **82**, 603–664 (2010).

[2] H. Ji, W. Daughton, J. Jara-Almonte, A. Le, A. Stanier, and J. Yoo, "Magnetic reconnection in the era of exascale computing and multiscale experiments," Nat. Rev. Phys. **4**, 263 (2022).

[3] H. Che, J. F. Drake, and M. Swisdak, "A current filamentation mechanism for breaking magnetic field lines during reconnection," Nature **474**, 184–187 (2011).

[4] H. Che, "How anomalous resistivity accelerates magnetic reconnection," Phys. Plasmas **24**, 082115 (2017).

[5] D. B. Graham, Y. V. Khotyaintsev, A. Vaivads, M. Andre, C. Norgren, J. Drake, P.-A. Linqvist, O. Le Contel, R. Ergun, D. Gershman, B. Giles, C. Russell, W. Magnes, J. Burch, R. Torbert, K.-J. Hwang, and K. Dokgo, "Direct observations of anomalous resistivity and diffusion in collisionless plasma," Nat. Commun. **13**, 2954 (2022).

[6] S. D. Bale, F. S. Mozer, and T. Phan, "Observation of lower hybrid drift instability in the diffusion region at a reconnecting magnetopause," Geophys. Res. Lett. **29**, 2180, https://doi.org/10.1029/2002GL016113 (2002).

[7] C. Norgren, A. Vaivads, Y. V. Khotyaintsev, and M. André, "Lower hybrid drift waves: Space observations," Phys. Rev. Lett. **109**, 055001 (2012).

[8] D. B. Graham, Y. V. Khotyaintsev, C. Norgren, A. Vaivads, M. André, S. Toledo-Redondo, P.-A. Lindqvist, G. T. Marklund, R. E. Ergun, W. R. Paterson, D. J. Gershman, B. L. Giles, C. J. Pollock, J. C. Dorelli, L. A. Avanov, B. Lavraud, Y. Saito, W. Magnes, C. T. Russell, R. J. Strangeway, R. B. Torbert, and J. L. Burch, "Lower hybrid waves in the ion diffusion and magnetospheric inflow regions," J. Geophys. Res. **122**, 517–533, https://doi.org/10.1002/2016JA023572 (2017).

[9] D. B. Graham, Y. V. Khotyaintsev, C. Norgren, A. Vaivads, M. André, J. F. Drake, J. Egedal, M. Zhou, O. L. Contel, J. M. Webster, B. Lavraud, I. Kacem, V. Génot, C. Jacquey, A. C. Rager, D. J. Gershman, J. L. Burch, and R. E. Ergun, "Universality of lower hybrid waves at Earth's magnetopause," J. Geophys. Res.: Space Phys. **124**, 8727–8760, https://doi.org/10.1029/2019JA027155 (2019).

[10] L.-J. Chen, S. Wang, M. Hesse, R. E. Ergun, T. Moore, B. Giles, N. Bessho, C. Russell, J. Burch, R. B. Torbert, K. J. Genestreti, W. Paterson, C. Pollock, B. Lavraud, O. Le Contel, R. Strangeway, Y. V. Khotyaintsev, and P.-A. Lindqvist, "Electron diffusion regions in magnetotail reconnection under varying guide fields," Geophys. Res. Lett. **46**, 6230–6238, https://doi.org/10.1029/2019GL082393 (2019).

[11] L.-J. Chen, S. Wang, O. Le Contel, A. Rager, M. Hesse, J. Drake, J. Dorelli, J. Ng, N. Bessho, D. Graham, L. B. Wilson, T. Moore, B. Giles, W. Paterson, B. Lavraud, K. Genestreti, R. Nakamura, Y. V. Khotyaintsev, R. E. Ergun, R. B. Torbert, J. Burch, C. Pollock, C. T. Russell, P.-A. Lindqvist, and L. Avanov, "Lower-hybrid drift waves driving electron nongyrotropic heating and vortical flows in a magnetic reconnection layer," Phys. Rev. Lett. **125**, 025103 (2020).

[12] J. Yoo, J.-Y. Ji, M. V. Ambat, S. Wang, H. Ji, J. Lo, B. Li, Y. Ren, J. Jara-Almonte, L.-J. Chen, W. Fox, M. Yamada, A. Alt, and A. Goodman, "Lower hybrid drift waves during guide field reconnection," Geophys. Res. Lett. **47**, e2020GL087192, https://doi.org/10.1029/2020GL087192 (2020).

[13] T. A. Carter, H. Ji, F. Trintchouk, M. Yamada, and R. M. Kulsrud, "Measurement of lower-hybrid drift turbulence in a reconnecting current sheet," Phys. Rev. Lett. **88**, 015001 (2001).

[14] H. Ji, S. Terry, M. Yamada, R. Kulsrud, A. Kuritsyn, and Y. Ren, "Electromagnetic fluctuations during fast reconnection in a laboratory plasma," Phys. Rev. Lett. **92**, 115001 (2004).

[15] J. Yoo, M. Yamada, H. Ji, J. Jara-Almonte, C. E. Myers, and L.-J. Chen, "Laboratory study of magnetic reconnection with a density asymmetry across the current sheet," Phys. Rev. Lett. **113**, 095002 (2014).

[16] J. Yoo, J. Ng, H. Ji, S. Bose, A. Goodman, A. Alt, L.-J. Chen, P. Shi, and M. Yamada, "Anomalous resistivity and electron heating by lower hybrid drift waves during magnetic reconnection with a guide field," Phys. Rev. Lett. **132**, 145101 (2024).

[17] P. H. Yoon and A. T. Y. Lui, "Lower-hybrid-drift and modified-two-stream instabilities in current sheet equilibrium," J. Geophys. Res. **109**, A02210, https://doi.org/10.1029/2003JA010180 (2004).

[18] R. Kulsrud, H. Ji, W. Fox, and M. Yamada, "An electromagnetic drift instability in the magnetic reconnection experiment and its importance for magnetic reconnection," Phys. Plasmas **12**, 082301 (2005).

[19] I. Silin, J. Büchner, and A. Vaivads, "Anomalous resistivity due to nonlinear lower-hybrid drift waves," Phys. Plasmas **12**, 062902 (2005).

[20] P. H. Yoon and A. T. Y. Lui, "Anomalous resistivity by fluctuation in the lower-hybrid frequency range," J. Geophys. Res.: Space Phys. **112**, A06207, https://doi.org/10.1029/2006JA012209 (2007).

[21] V. Roytershteyn, W. Daughton, H. Karimabadi, and F. S. Mozer, "Influence of the lower-hybrid drift instability on magnetic reconnection in asymmetric configurations," Phys. Rev. Lett. **108**, 185001 (2012).

[22] V. Roytershteyn, S. Dorfman, W. Daughton, H. Ji, M. Yamada, and H. Karimabadi, "Electromagnetic instability of thin reconnection layers: Comparison of three-dimensional simulations with MRX observations," Phys. Plasmas **20**, 061212 (2013).

[23] R. Davidson, N. Gladd, C. Wu, and J. Huba, "Effects of finite plasma beta on the lower-hybrid drift instability," Phys. Fluids **20**, 301 (1977).

[24] N. Ahmadi, H. Ji, J. Yoo, R. Ergun, I. Thomas, R. Banka, E. Schultz-Stachnik, and A. Alex, "Properties of lower hybrid drift waves and energy transfer near and inside the magnetic reconnection electron diffusion regions," J. Geophys. Res.: Space Phys. **130**, e2024JA033238, https://doi.org/10.1029/2024JA033238 (2025).

[25] F. S. Mozer, M. Wilber, and J. F. Drake, "Wave associated anomalous drag during magnetic field reconnection," Phys. Plasmas **18**, 102902 (2011).

[26] Y. Ren, L. Dai, C. Wang, and B. Lavraud, "Statistical properties of lower hybrid waves in the magnetopause reconnection exhaust region," J. Geophys. Res.: Space Phys. **128**, e2022JA031242, https://doi.org/10.1029/2022JA031242 (2023).

[27] J. Yoo, Y. Hu, J.-Y. Ji, H. Ji, M. Yamada, A. Goodman, K. Bergstedt, W. Fox, and A. Alt, "Effects of coulomb collisions on lower hybrid drift waves inside a laboratory reconnection current sheet," Phys. Plasmas **29**, 022109 (2022).

[28] M. Yamada, H. Ji, S. Hsu, T. Carter, R. Kulsrud, N. Bretz, F. Jobes, Y. Ono, and F. Perkins, "Study of driven magnetic reconnection in a laboratory plasma," Phys. Plasmas **4**, 1936–1944 (1997).

[29] J. Yoo, B. Na, J. Jara-Almonte, M. Yamada, H. Ji, V. Roytershteyn, M. R. Argall, W. Fox, and L.-J. Chen, "Electron heating and energy inventory during asymmetric reconnection in a laboratory plasma," J. Geophys. Res.: Space Phys. **122**, 9264–9281, https://doi.org/10.1002/2017JA024152 (2017).

[30] Y. Hu, J. Yoo, H. Ji, A. Goodman, and X. Wu, "Probe measurements of electric field and electron density fluctuations at megahertz frequencies using in-shaft miniature circuits," Rev. Sci. Instrum. **92**, 033534 (2021).

[31] H. Ji and W. Daughton, "Phase diagram for magnetic reconnection in heliophysical, astrophysical, and laboratory plasmas," Phys. Plasmas **18**, 111207 (2011).

[32] H. Ji, R. Kulsrud, W. Fox, and M. Yamada, "An obliquely propagating electromagnetic drift instability in the lower hybrid frequency range," J. Geophys. Res. **110**, A08212, https://doi.org/10.1029/2005JA011188 (2005).

[33] J. Yoo, M. Yamada, H. Ji, J. Jara-Almonte, and C. E. Myers, "Bulk ion acceleration and particle heating during magnetic reconnection in a laboratory plasma," Phys. Plasmas **21**, 055706 (2014).

[34] J. Yoo, J. Jara-Almonte, E. Yerger, S. Wang, T. Qian, A. Le, H. Ji, M. Yamada, W. Fox, E.-H. Kim, L.-J. Chen, and D. J. Gershman, "Whistler wave generation by anisotropic tail electrons during asymmetric magnetic reconnection in space and laboratory," Geophys. Res. Lett. **45**, 8054–8061, https://doi.org/10.1029/2018GL079278 (2018).

[35] J. Ng, J. Yoo, L.-J. Chen, N. Bessho, and H. Ji, "3D simulation of lower-hybrid drift waves in strong guide field asymmetric reconnection in laboratory experiments," Phys. Plasmas **30**, 042101 (2023).

[36] R. Davidson, N. Gladd, C. Wu, and J. Huba, "Influence of finite-β effects on the lower-hybrid drift instability in post-implosion θ pinches," Phys. Rev. Lett. **37**, 750 (1976).

[37] A. v Stechow, W. Fox, J. Jara-Almonte, J. Yoo, H. Ji, and M. Yamada, "Electromagnetic fluctuations during guide field reconnection in a laboratory plasma," Phys. Plasmas **25**, 052120 (2018).

[38] J. Yoo, S. Wang, E. Yerger, J. Jara-Almonte, H. Ji, M. Yamada, L.-J. Chen, W. Fox, A. Goodman, and A. Alt, "Whistler wave generation by electron temperature anisotropy during magnetic reconnection at the magnetopause," Phys. Plasmas **26**, 052902 (2019).

[39] H. Tanabe, T. Yamada, T. Watanabe, K. Gi, K. Kadowaki, M. Inomoto, R. Imazawa, M. Gryaznevich, C. Michael, B. Crowley, N. J. Conway, R. Scannell, J. Harrison, I. Fitzgerald, A. Meakins, N. Hawkes, K. G. McClements, T. O'Gorman, C. Z. Cheng, Y. Ono, and MAST Team, "Electron and ion heating characteristics during magnetic reconnection in the mast spherical tokamak," Phys. Rev. Lett. **115**, 215004 (2015).

[40] I. H. Cairns and B. F. McMillan, "Electron acceleration by lower hybrid waves in magnetic reconnection regions," Phys. Plasmas **12**, 102110 (2005).

[41] J. L. Burch, R. B. Torbert, T. D. Phan, L.-J. Chen, T. E. Moore, R. E. Ergun, J. P. Eastwood, D. J. Gershman, P. A. Cassak, M. R. Argall, S. Wang, M. Hesse, C. J. Pollock, B. L. Giles, R. Nakamura, B. H. Mauk, S. A. Fuselier, C. T. Russell, R. J. Strangeway, J. F. Drake, M. A. Shay, Y. V. Khotyaintsev, P.-A. Lindqvist, G. Marklund, F. D. Wilder, D. T. Young, K. Torkar, J. Goldstein, J. C. Dorelli, L. A. Avanov, M. Oka, D. N. Baker, A. N. Jaynes, K. A. Goodrich, I. J. Cohen, D. L. Turner, J. F. Fennell, J. B. Blake, J. Clemmons, M. Goldman, D. Newman, S. M. Petrinec, K. J. Trattner, B. Lavraud, P. H. Reiff, W. Baumjohann, W. Magnes, M. Steller, W. Lewis, Y. Saito, V. Coffey, and M. Chandler, "Electron-scale measurements of magnetic reconnection in space," Science **352**, aaf2939 (2016).

[42] M. Hesse, K. Schindler, J. Birn, and M. Kuznetsova, "The diffusion region in collisionless magnetic reconnection," Phys. Plasmas **6**, 1781–1795 (1999).

[43] R. B. Torbert, J. L. Burch, T. D. Phan, M. Hesse, M. R. Argall, J. Shuster, R. E. Ergun, L. Alm, R. Nakamura, K. J. Genestreti, D. J. Gershman, W. R. Paterson, D. L. Turner, I. Cohen, B. L. Giles, C. J. Pollock, S. Wang, L.-J. Chen, J. E. Stawarz, J. P. Eastwood, K. J. Hwang, C. Farrugia, I. Dors, H. Vaith, C. Mouikis, A. Ardakani, B. H. Mauk, S. A. Fuselier, C. T. Russell, R. J. Strangeway, T. E. Moore, J. F. Drake, M. A. Shay, Y. V. Khotyaintsev, P.-A. Lindqvist, W. Baumjohann, F. D. Wilder, N. Ahmadi, J. C. Dorelli, L. A. Avanov, M. Oka, D. N. Baker, J. F. Fennell, J. B. Blake, A. N. Jaynes, O. L. Contel, S. M. Petrinec, B. Lavraud, and Y. Saito, "Electron-scale dynamics of the diffusion region during symmetric magnetic reconnection in space," Science **362**, 1391–1395 (2018).

[44] J. Yoo (2025). "Anomalous resistivity and electron heating by lower hybrid drift waves inside reconnecting current sheets," Princeton Data Commons. https://doi.org/10.34770/hrkt-rw14